© 2019. Published by The Company of Biologists Ltd | Journal of Cell Science (2019) 132, jcs230672. doi:10.1242/jcs.230672

RESEARCH ARTICLE

The golgin *Pp*Imh1 mediates reversible cisternal stacking in the Golgi of the budding yeast *Pichia pastoris*

Bhawik Kumar Jain[1,2], Roma Dahara[1,2] and Dibyendu Bhattacharyya[1,2,*]

ABSTRACT

The adhesive force for cisternal stacking of Golgi needs to be reversible – to be initiated and undone in a continuous cycle to keep up with the cisternal maturation. Microscopic evidence in support of such a reversible nature of stacking, in the form of 'TGN peeling,' has been reported in various species, suggesting a potential evolutionarily conserved mechanism. However, knowledge of such mechanism has remained sketchy. Here, we have explored this issue in the budding yeast *Pichia pastoris* which harbors stacked Golgi. We observed that deletion of GRIP domain golgin *P. pastoris* (*Pp*)*IMH1* increases the peeling of late cisterna, causing unstacking of the Golgi stack. Our results suggest that the *Pp*Imh1 dimer mediates reversible stacking through a continuous association–dissociation cycle of its GRIP domain to the middle and late Golgi cisterna under the GTP hydrolysis-based regulation of Arl3-Arl1 GTPase cascade switch. The reversible cisternal stacking function of *Pp*Imh1 is independent of its vesicle-capturing function. Since GRIP domain proteins are conserved in plants, animals and fungi, it is plausible that this reversible mechanism of Golgi stacking is evolutionarily conserved.

This article has an associated First Person interview with the first author of the paper.

KEY WORDS: Cisternal stacking, GRIP domain, Golgi, Golgin, *Pp*Imh1

INTRODUCTION

The Golgi plays a centralized role in the processing, sorting and secretion of various cargo molecules destined for various intracellular and extracellular destinations (Nakamura et al., 2012). The Golgi display variable shape in different species: from dispersed cisternae in *Saccharomyces cerevisiae* to stacked cisternal structures in *Pichia pastoris* and to laterally connected ribbon of cisternal stacks in vertebrates. However, the mechanisms that regulate such exotic organizations are still poorly understood (Lowe, 2011; Papanikou and Glick, 2009).

In the light of the cisternal maturation model, the cisternal stacking of the Golgi needs to be reversible – to be initiated and undone in a continuous cycle to keep up with the cycle of cisternal maturation. Microscopic evidence in support of such reversible nature of the cisternal stacking has been reported. Trans-Golgi network (TGN) elements have been shown to peel off from Golgi stacks in various species ranging from *P. pastoris* to plants to mammals (Mogelsvang et al., 2003; Mollenhauer and Morré, 1991). These well-documented results point to a potential evolutionarily conserved regulatory mechanism of reversible stacking. However, mechanistically, nothing is known about such reversible stacking to date.

The most well-known factors that have been reported to play a role in cisternal stacking are GRASP proteins. Double knockout of GRASPs in mammalian cells (GRASP55 and GRASP65, also known as GORASP2 and GORASP1, respectively) disperses the Golgi ribbon structure into individual cisternae and tubulovesicular structures (Bekier et al., 2017). GRASPs are peripheral membrane proteins on the cytoplasmic face of the Golgi cisternae that form trans-oligomers through their N-terminal GRASP domain and thereby adhere adjacent cisternae together into a stack and link Golgi stacks into a ribbon, suggesting oligomerization as a mechanism of cisternal stacking (Zhang and Wang, 2015). However, no regulatory on–off switch that regulates the cisternal stacking function of the GRASPs to accommodate the reversible stacking theory has yet been discovered.

Moreover, the primary functions of GRASPs are not at all conserved among different species. In the budding yeast *P. pastoris* deletion of the GRASP homolog GRH1 does not affect Golgi stacking, and plant cells apparently have no identifiable GRASP homolog (Levi et al., 2010; Ito et al., 2014). These studies suggest that GRASP homologs are not functionally conserved regarding Golgi stacking in species that evidently displays stacked Golgi. Such observation indicates that other Golgi factors could mediate regulated adhesive interaction necessary for the cisternal stacking.

The golgins are long coiled-coil domain proteins that have been shown to be necessary for the maintenance of the Golgi structure and vesicle tethering (Ramirez and Lowe, 2009). The discovery of the golgins coincided with the observation that Golgi membranes could be extracted with detergent to leave a proteinaceous matrix that retained the organization of Golgi cisternae. Golgins such as GM130/golgin-95 (also known as GOLGA2) and p115 (also known as USO1) were found to be components of this matrix, and with their elongated structure, it was suggested that golgins function in the maintenance and establishment of Golgi structure (Slusarewicz et al., 1994; Nakamura et al., 1995; Waters et al., 1992). Knockdown of Golgin-97, Golgin-245 and GCC185 (also known as GOLGA1, GOLGA4 and GCC2, respectively) have been shown to affect the Golgi structure, suggesting a role for golgins in Golgi structure maintenance (Lu et al., 2004; Derby et al., 2007; Alzhanova and Hruby, 2006). Recently it has been reported that efficient stacking occurs in the absence of GRASP65 and/or GRASP55 when either of these two golgins is overexpressed (Lee et al., 2014). This result suggests that golgins serve as potential alternative cisternal adhesive factors.

[1]Department of Cell and Tumor Biology, Advanced Centre for Treatment Research & Education in Cancer (ACTREC), Tata Memorial Centre, Kharghar, Navi Mumbai, 410210 MH, India. [2]Homi Bhabha National Institute, Training School Complex, Anushakti Nagar, Mumbai, MH 400085, India.

*Author for correspondence (dbhattacharyya@actrec.gov.in)

B.K.J., 0000-0002-1362-6139; R.D., 0000-0003-3841-3436; D.B., 0000-0003-3252-7440

Received 5 February 2019; Accepted 22 July 2019

Journal of Cell Science (2019) 132, jcs230672. doi:10.1242/jcs.230672

GRIP-domain-containing golgins associate and dissociate with the Golgi in a GTP-dependent manner (Setty et al., 2003; Wu et al., 2004). In this study, we have tested the role of the GRIP domain golgin *Pp*Imh1p in the Golgi structure in the budding yeast *P. pastoris*. *P. pastoris* provides an excellent model to study cisternal stacking as we can study the individual Golgi stack and adhesion between two individual Golgi cisternae. We observed that deletion of *P. pastoris* GRIP domain golgin *PpIMH1* dramatically increases the peeling of late cisterna, causing partial unstacking from the rest of the Golgi stack. Deletion of the *PpIMH1* dimerization motif, overexpression of its GRIP domain alone, deletion mutants of *arl1* or *arl3*, and a GDP-locked *arl3* mutant also show a similar phenotype. We have shown the evolutionarily conserved GRIP domain golgin *Pp*Imh1 mediates reversible stacking between medial and late cisterna, and this mechanism is regulated by the Arl3–Arl1 GTPase cascade switch.

RESULTS

Golgin *PpIMH1* deletion affects cisternal stacking

We wanted to investigate the potential roles of GRIP-domain-containing golgins in mediating cisternal stacking in budding yeast. In the budding yeast *P. pastoris,* the only GRIP-domain-containing golgin is *Pp*Imh1 (Jain et al., 2018). We here test whether the deletion of *Pp*Imh1 has any effect on cisternal stacking. To study cisternal stacking, we decided to create a *Pichia* strain in which early Golgi compartment and late Golgi compartments are labeled with two different fluorescent protein fusions. For studies in *S. cerevisiae*, our lab, as well as other groups, has used fluorescently tagged versions of the early Golgi protein VRG4 and the late Golgi protein Sec7 to mark early and late Golgi compartments, respectively (Bhave et al., 2014; Iyer et al., 2018; Losev et al., 2006). For our *Pichia* assay system, we created a strain in which the early Golgi protein VIG4 is tagged with msGFP, and late Golgi protein SEC7 is tagged with DsRed.M1x6 (hereafter referred to as the two-color Golgi strain). Live cells were imaged by fluorescence confocal microscopy. Golgi cisternae were visualized both with 2D projections along with 3D rendering, for quantitative measurements. In wild-type cells, we observe that GFP–VIG4 and SEC7–DsRed.M1x6 show elongated green and red signal, respectively, representing early and late cisterna stacked in close proximity resulting in a 'traffic light' type of juxtaposed signal (Fig. 1A). The green and red signals are very close and almost

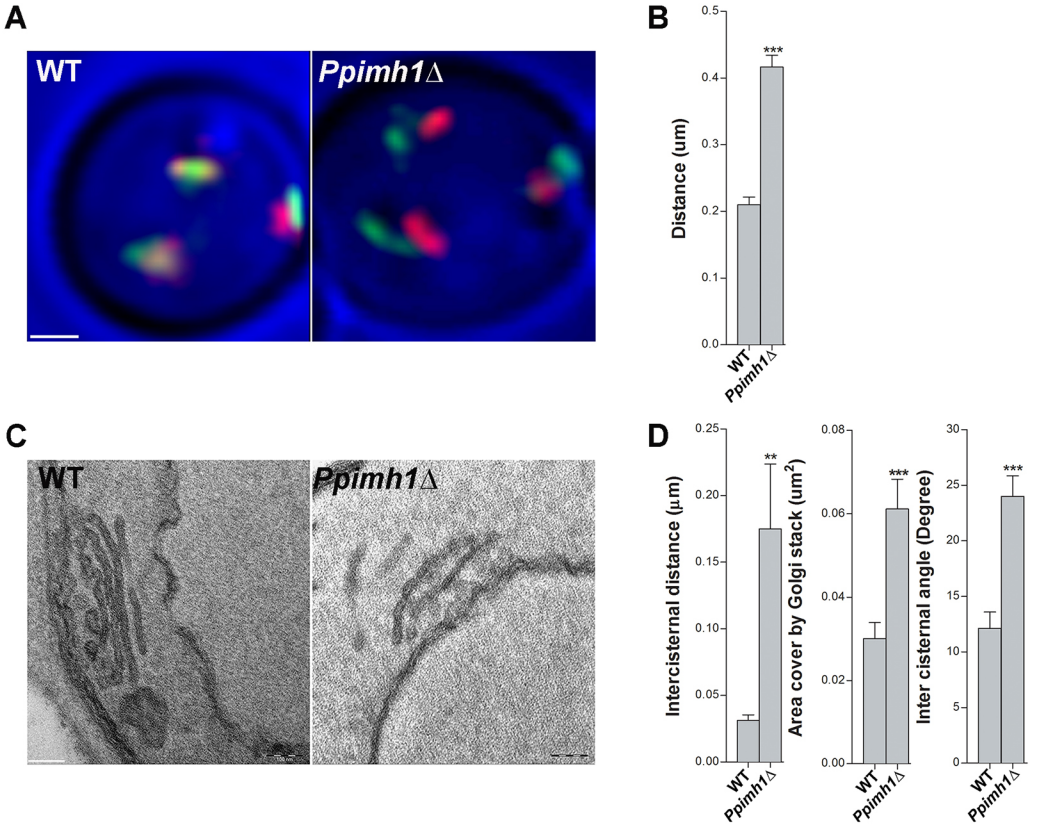

Fig. 1. Inter-cisternal distance is significantly increased in *Ppimh1*Δ cells. (A) Wild-type (WT) *P. pastoris* cells expressing msGFP-*VIG4* and *SEC7*-DsRed.M1x6 or the same cells where *PpIMH1* was deleted (*Ppimh1*Δ) were grown in YPD medium to log phase and imaged under a Zeiss LSM780 confocal microscope. Optical sections of 200 nm thickness were collected for the entire volume of cells. The image hyperstack was deconvoluted using Huygens Pro and further filtered and *Z*-projected using ImageJ. Representative cells are shown. Scale bar: 1 µm. (B) The distance between the green and red spot was measured using Imarisx64 8.0.1 Biplane. To quantify the inter-cisternal distance, images were opened in Imaris, the surface was filled using 3D rendering for a specific channel, then the individual surface was considered as a solid object, and the center point was selected. By using the pointer, the distance between one green and one red spot was measured. Values represent mean±s.e.m. (*n*=60 cells). ****P*<0.0006 (Student's *t*-test). (C) Thin-section electron micrographs where taken for wild-type and *Ppimh1*Δ PPY12 cells as described in the Materials and Methods. Representative cells are shown. Scale bar: 100 nm. (D) Quantitative data from thin section electrographs measured using iTEM software. The maximum inter-cisternal distance between two cisternae was measured by drawing a line between the medial Golgi and TGN. The total area covered by the entire Golgi stack was measured by drawing a shape covering entire Golgi stack area. The angle between two cisternae was measured by drawing a line on medial Golgi and TGN, and angle between the two lines was measured. Values represent mean±s.e.m. (*n*=45 cells). ***P*=0.0016; ****P*<0.0006 (Student's *t*-test).

Journal of Cell Science (2019) 132, jcs230672. doi:10.1242/jcs.230672

located on the top of each other. However, deletion of the golgin *Pp*Imh1 results in a clear separation of these green and red signals, allowing each cisterna to be visualized distinctly with no apparent overlap (Fig. 1A). This result suggests that *Pp*Imh1 deletion causes a slight separation between Golgi cisternal stacks, which was confirmed by quantitative measurements of the distance between the center of green and red spots achieved through 3D rendering (Fig. 1B). To gain further insight into structural details, we resorted to electron microscopy of *Ppimh1*Δ cells along with wild-type cells, as a control. Electron microscopy (EM) data show that there is a clear increase in the inter-cisternal distance between medial and late Golgi compartments in *Ppimh1*Δ cells (Fig. 1C). It appears, in the majority of the cells, that the TGN is positioned at an angle to the Golgi stack with only one of its ends attached to the rest of the stack. To quantitatively characterize this mutant phenotype, we have measured several parameters from the EM micrographs (Fig. 1D). We found that the inter-cisternal angle between TGN and medial Golgi was increased in *Ppimh1*Δ strain as compared to the wild-type. Moreover, the total area covered by the entire Golgi stack was also increased. These experiments indicate that *Pp*Imh1 deletion affects cisternal stacking of Golgi and possibly between medial and late Golgi compartments.

The coiled-coil domain of *PpIMH1* is essential for the cisternal stacking function *PpIMH1*

PpIMH1 contains an N-terminal head domain, Golgi-localizing C-terminal GRIP domain and long central coiled-coil domains (Munro and Nichols, 1999). Through a two-hybrid analysis, we have previously provided direct evidence that coiled coil domain of PpImh1 can mediate self-dimerization (Jain et al., 2018). The long coiled-coil domains could potentially mediate dimerization of golgin molecules residing on two different Golgi cisterna and multiple such dimerized golgin pairs could bring Golgi cisternae together to form a stack. To test this hypothesis, we need to test whether the coiled-coil domain is essential for cisternal stacking or not. According to coiled-coil domain analysis, the central region of *Pp*Imh1 (residues 150–1070) is likely to form a coiled-coil structure (Fig. S1) (Jain et al., 2018). Full-length *Pp*Imh1 was fully competent to rescue the unstacking phenotype of *Pp*Imh1Δ cells, but *Pp*Imh1Δ(150-1070) was not able to rescue the unstacking phenotype (Fig. 2). *Pp*Imh1(150-1070)Δ localizes to the Golgi (Fig. S2). Cells with a deletion of the *Pp*Imh1(150-1070) coiled-coil domain from the endogenous *P*pIMH1 in the background of the two-color Golgi strain displayed a similar cisternal unstacking phenotype (Fig. 2C). We also found that the inter-cisternal distance, area cover by the entire Golgi stack and inter-cisternal angle increase in the PPY12-*Pp*Imh1(150-1070)Δ strain (Fig. 2D). Along with previously demonstrated direct evidence of self-dimerization capabilities of *Pp*Imh1 the coiled-coiled domain (Jain et al., 2018), these results suggest that *Pp*Imh1(150-1070), which has shown a high probability to form a coiled-coil domain, is essential for the cisternal stacking function of *Pp*Imh1.

Overexpression of the the *Pp*Imh1 GRIP domain results in a cisternal unstacking phenotype

The GRIP domain of TGN golgins acts as a Golgi-localizing signal. A GRIP domain tagged with GFP is known to localize to the late Golgi/TGN in yeast and mammalian cells. In addition, overexpression of a GRIP domain causes a dominant-negative like phenotype by competing with endogenous GRIP-domain-containing proteins for binding to Arl1 (Munro and Nichols, 1999; Setty et al., 2003; Lu et al., 2004). If *Pp*Imh1 is indeed mediating the cisternal stacking through dimerization of coiled-coil regions, then it is conceivable that the overexpression of GRIP domains would saturate all the binding sites in *Pp*Imh1. Accordingly, such overexpression in *P. pastoris* cells might cause cisternal unstacking as dominant-negative-like phenotype as most of the endogenous *Pp*Imh1 would not be localized to the Golgi. To test this hypothesis, we overexpressed the GRIP domain under the methanol-inducible AOX1 promoter; this indeed resulted in a cisternal unstacking phenotype (Fig. 3A). We observed that GRIP domain overexpression resulted in an increase in the inter-cisternal distance, the area cover by the entire Golgi stack and inter-cisternal angle (Fig. 3B). However, similar overexpression of the coiled-coil domain did not show any effect on cisternal stacking (Fig. 3A,B). To understand the localization of these overexpressed domains, we tagged the GRIP domain (*Pp*-GRIP domain) and coiled-coil (*Pp*-CC) domain with GFP, and expressed them under the control of AOX1 promoter. Western blot analysis confirmed that these fusions were stably expressed and were free from any proteolytic degradation (Fig. S2C). We observed that overexpressed *Pp*-GRIP domain showed a typical punctate Golgi pattern, while overexpressed *Pp*-CC, which lacks a GRIP domain, failed to localize to the Golgi and instead was accumulated in cytosol (Fig. S2B). Hence, we conclude that overexpression of the coiled-coil domain alone did not affect cisternal stacking owing to the lack of Golgi localization of the overexpressed fusion protein. This result also suggests that although the coiled-coil domain may be essential for cisternal stacking, it is itself not sufficient to confer the cisternal stacking function, because it requires the GRIP domain to localize to Golgi. It is to be noted that GRIP domain overexpression in mammalian cells causes disruption in Golgi morphology and substantially affects TGN architecture (Yoshino et al., 2003). Taken together, all these results support our hypothesis and potential conservative nature of function of the GRIP domain of golgin in cisternal stacking.

The Arl1–Arl3 GTPase cascade switch regulates the cisternal unstacking phenotype

Yeast Arl1 and Arl3 are divergent members of the ARF family of GTPases, referred to as ARF-like or ARL GTPases, and they show a high level of conservation with the human ARL1 and ARF-related protein (ARP) GTPases, respectively. Arl1-GTP interacts with the GRIP domain, and this interaction regulates the Golgi recruitment of Golgin-97, the mammalian homolog of Imh1. In the budding yeast *S. cerevisiae*, Arl1–Arl3 works in cascade, whereby the GTPase cycle of Arl3 regulates the Golgi localization of Arl1, which in turn binds to the GRIP domain of Imh1 and recruits it to the Golgi. Arl3 and Arl1 are reported to be receptors for the GRIP domain proteins (Lu and Hong, 2003; Panic et al., 2003; Setty et al., 2003). To validate this in *P. pastoris*, we tagged the chromosomal locus of *PpIMH1* with GFP and transformed into wild-type and *arl3*Δ strains separately. GFP–Imh1 was found to be localized throughout the cytoplasm in case of *arl3*Δ cells, whereas in the wild-type it was localized to the Golgi (Fig. S3A). A similar result was previously observed with the *arl1*Δ strain (Jain et al., 2018). Together, these results suggest that the roles of both ARL3 and ARL1 are functionally conserved. We also determined the localization of GFP–*Pp*Imh1 in strains with GDP-locked Arl3 (T31N). We observed that the GFP–*Pp*Imh1 signal mostly localized to the cytosol, suggesting that the GTP-GDP-association-based regulatory role of Arl3–Arl1 GTPase cascade switch for PpImh1 recruitment to Golgi is also conserved (Fig. S3B).

Since the recruitment of *Pp*Imh1 to the Golgi is dependent on the function of Arl3–Arl1, we hypothesize that deletion of either

Journal of Cell Science (2019) 132, jcs230672. doi:10.1242/jcs.230672

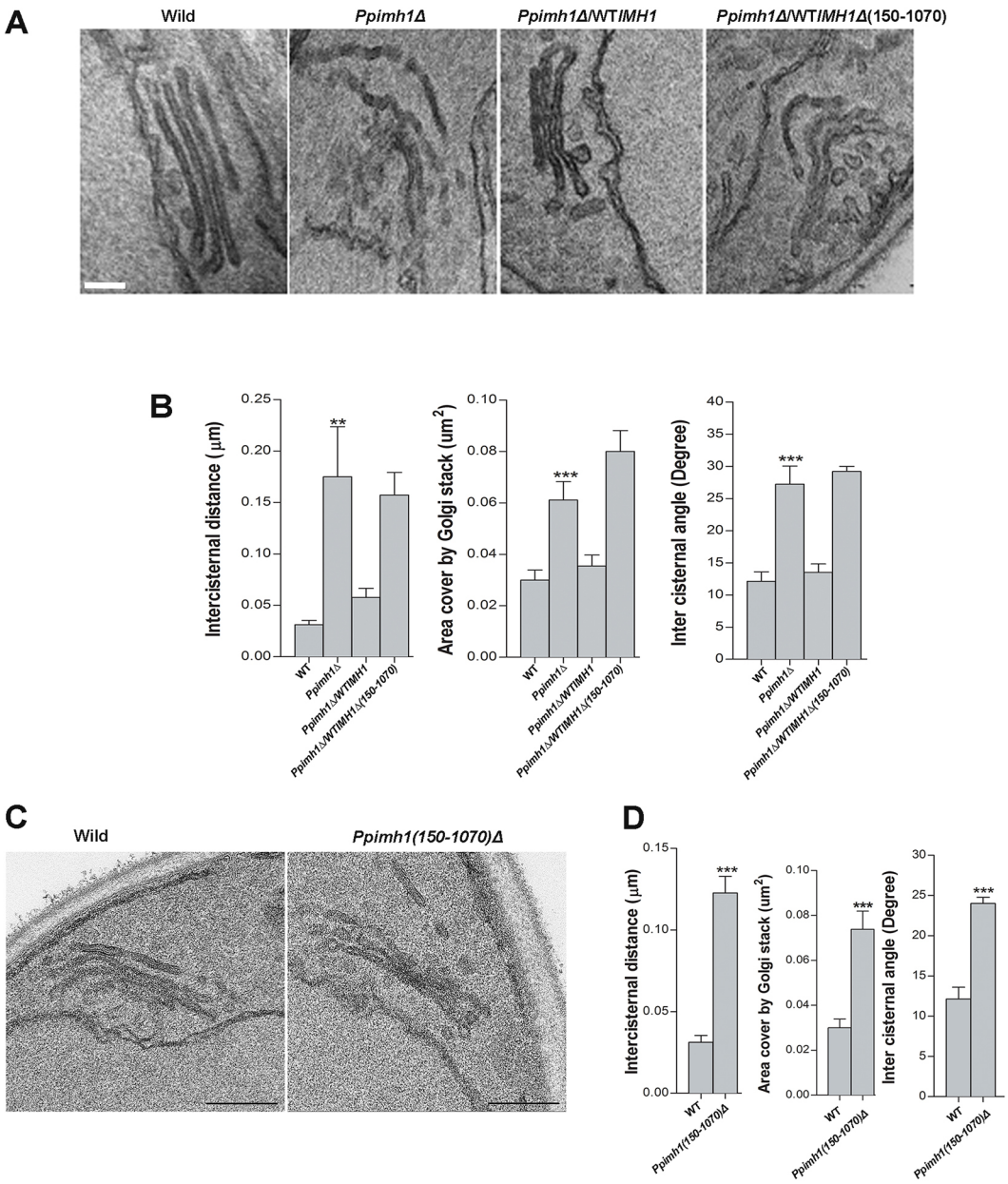

Fig. 2. Full-length *PpIMH1* could rescue the *Ppimh1*Δ deletion phenotype, but a version *PpImh1* lacking the coiled-coil domain fails to rescue this phenotype. (A) Thin-section electron micrographs of wild-type cells (wild), *Ppimh1Δ* cells and *Ppimh1Δ* cells transformed with full-length *PpIMH1* (*Ppimh1Δ*/WT*IMH1*) and *PpImh1*Δ(150-1070) [*Ppimh1Δ*/WT*IMH1*Δ(150-1070)], The *Ppimh1Δ* strain was transformed with full-length *PpIMH1* and *PpImh1*Δ(150-1070) as a second copy. All the strains were grown until log phase; then cells were concentrated, fixed and stained. Cells were embedded in Spurr's resin, then sections were taken and observed under an electron microscope. Representative cells are shown. Scale bar: 100 nm. (B) Quantitative data from thin section electrograph were measured using iTEM analysis software. Left, maximum intercisternal distance between two cisternae; middle, area covered by the entire Golgi stack; right, angle between two cisternae. Values represent mean±s.e.m. (*n*=45 cells). ***P*=0.0016; ****P*<0.003 (Student's *t*-test). (C) Thin section electron micrographs of *P. pastoris* PPY12 wild-type and *PpIMH1*(150-1070)Δ coiled-coil domain deletion strains were taken as described in the Materials and Methods. A representative cell is shown. Scale bar: 100 nm. (D) Quantitative data from thin section electrographs were measured using iTEM analysis software. Left, maximum intercisternal distance between two cisternae; middle, area covered by the entire Golgi stack; right, angle between two cisternae. Values represent mean±s.e.m. (*n*=45 cells). ****P*<0.0001 (Student's *t*-test).

arl3 or *arl1* in *P. pastoris* cells should result in a similar cisternal unstacking phenotype to that seen when *Pp*Imh1 is deleted. To test that, we created *arl3*Δ and *arl1*Δ strains in the background of the two-color Golgi strain. Indeed, we observed a cisternal unstacking phenotype in both the strains both through light microscopy and electron microscopy (Fig. 4A,B). There was an increase in inter-cisternal distance, area cover by the entire Golgi stack and inter-cisternal angle (Fig. 4C). These results once again strengthen our hypothesis that *Pp*Imh1 is indeed mediating the cisternal stacking of Golgi.

The cisternal maturation model suggests that early cisterna mature into late cisterna and the late compartment/TGN 'peels' away from the stack (Mogelsvang et al., 2003). The repeated cycle of cisternal maturation needs to be continued to maintain the Golgi cisternal stack, which suggests that cisternal stacking needs to be reversible. Arl3–Arl1 works in coordination, so that the GTPase cycle of Arl3

Journal of Cell Science (2019) 132, jcs230672. doi:10.1242/jcs.230672

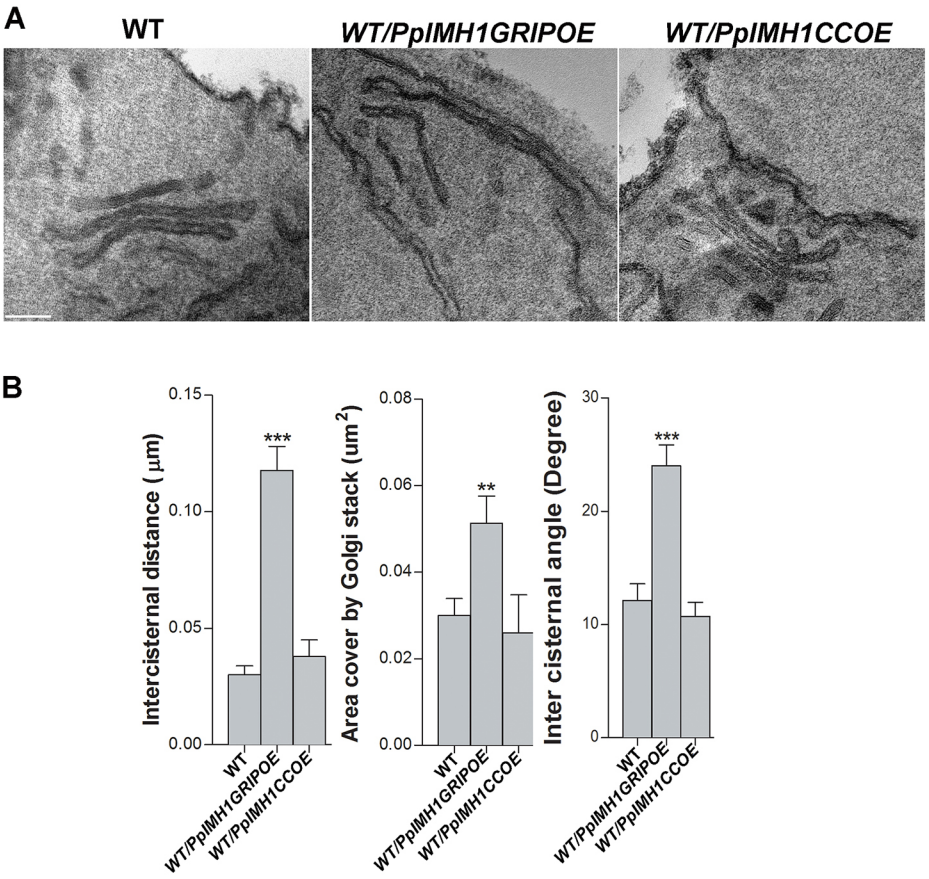

Fig. 3. Overexpression of *Pp*Imh1 GRIP domain alone can cause unstacking phenotype while overexpression of only *Pp*Imh1 coiled-coil domain alone causes no such effect. (A) Thin-section electron micrograph of a wild-type (WT) cell *P. pastoris* and cells overexpressing with the *Pp*Imh1 GRIP domain (WT/PpIMH1GRIPOE) and coiled-coil domain (WT/PpIMH1CCOE). *PpIMH1GRIP* and *PpIMH1CC* were cloned in a pIB4 vector under the control of the methanol-inducible promoter AOX1. Cells were grown until the log phase in SYG (glycerol) and overexpression was induced with 1% methanol. Cells were concentrated, fixed, and processed for thin section electron micrograph as described in the Materials and Methods. Representative cells are shown. Scale bar: 100 nm. (B) Quantitative data from thin section electrographs were measured using iTEM analysis software. Left, maximum intercisternal distance between two cisternae; middle, area covered by the entire Golgi stack; right, angle between two cisternae. Values represent mean±s.e.m. (*n*=45 cells). ***P*=0.0057; ****P*<0.005 (Student's *t*-test).

regulates Golgi localization of Arl1, and that, in turn, binds to the GRIP domain of *Pp*Imh1p and recruits it to the Golgi. It is expected that the Arl3–Arl1 GTPase cascade, through its GTP hydrolysis cycle, functions as an oscillatory regulatory switch for association and dissociation of *Pp*Imh1 to the Golgi, and thereby regulates its function in reversible stacking. In the absence of this regulation, or in the absence of *Pp*Imh1 itself, it would be expected that such reversible stacking would be lost, resulting in faster TGN peeling. To test this concept, we captured 4D live cell movies of the *arl3*Δ strain (Movie 4; Fig. 4D) along with wild-type cells (Movie 1, Fig. S4). 4D movies of *arl3*Δ, harboring two-color Golgi cisterna, shows that these cells have increased TGN peeling (Fig. S5). TGN peeling events occur (as red-labeled late cisterna that are be seen to peel off from the cisternal stack) and new red late cisterna can subsequently be seen maturing. We also captured live-cell 4D movies of *Ppimh*Δ (Movie 2) and *arl1*Δ (Movie 3) mutant strains, as well as movies from cells expressing the GDP-locked version of Arl3 (Arl3T31N) (Movie 5). All strains showed a significant increase in the TGN peeling frequency as compared to wild type (Fig. S5). These results suggest that *Pp*Imh1 indeed mediates the reversible stacking function, which is regulated by the Arl3–Arl1 GTPase cascade switch. The GTP hydrolysis cycle of the Arl proteins regulates *Pp*Imh1 association and dissociation to Golgi cisterna and thereby functions as an on-off switch for the stacking function of *Pp*Imh1 in a periodic manner.

*Pp*Imh1 is required for endosome to TGN trafficking

Knockdown of individual mammalian GRIP domain proteins has been reported to cause defects in the retrograde trafficking of some cargo proteins from endosomes to the TGN (Derby et al., 2007; Lu et al., 2004). Golgin-97, the mammalian homolog of *Pp*Imh1 has been implicated in recycling endosome trafficking (Burguete et al., 2008; Lu et al., 2004).

To test whether deletion of *Pp*Imh1 has any effect on endosome to TGN trafficking, we tagged, with GFP, the cargo protein Vps10, which shuttles between pre-vacuolar endosome and late Golgi/TGN. Vps10 functions as a sorting receptor in the Golgi compartments for transport and sorting of vacuolar proteins like CPY. Vps10 cycles between the late Golgi and pre-vacuolar endosome compartment (Cooper and Stevens, 1996; Marcusson et al., 1994). We checked the localization of Vps10–GFP in wild-type *P. pastoris* cells, which shows that Vps10 localized to compartments labeled by late Golgi marker Sec7 (Fig. 5A). Furthermore, we checked the localization of Vps10–GFP in *Ppimh1*Δ and *Ppimh1*(150-1070)Δ cells. In the case of *Ppimh1*Δ as well as *Ppimh1*(150-1070)Δ cells, Vps10 was not localized to the late Golgi (Fig. 5A). To further confirm the localization of Vps10 in *Pp*imh1Δ and *Pp*imh1(150-1070)Δ strains, we checked the localization of Vps10 with respect to FM-4-64, a dye previously shown to mark pre-vacuolar endosomal compartments (Bhave et al., 2014; Day et al., 2018). We also undertook a kinetics experiment to standardize the optimal exposure of endosomal compartments label FM-4-64 in *P. pastoris* (Fig. S6B). We observed that in wild-type cells, majority of Vps10 molecules localized to compartments marked by late Golgi marker Sec7 (Fig. 5B), but in case of *Pp*imh1Δ and *Ppimh1*(150-1070)Δ strains, localization of Vps10 increased in pre-vacuolar endosome compared to wild-type (Fig. S6A). This suggests that *PpImh1* deletion affects the pre-vacuolar endosome to late Golgi/TGN trafficking.

A short well-conserved region at the N-terminus of TGN golgins has been shown to be necessary and sufficient to nucleate the

Journal of Cell Science (2019) 132, jcs230672. doi:10.1242/jcs.230672

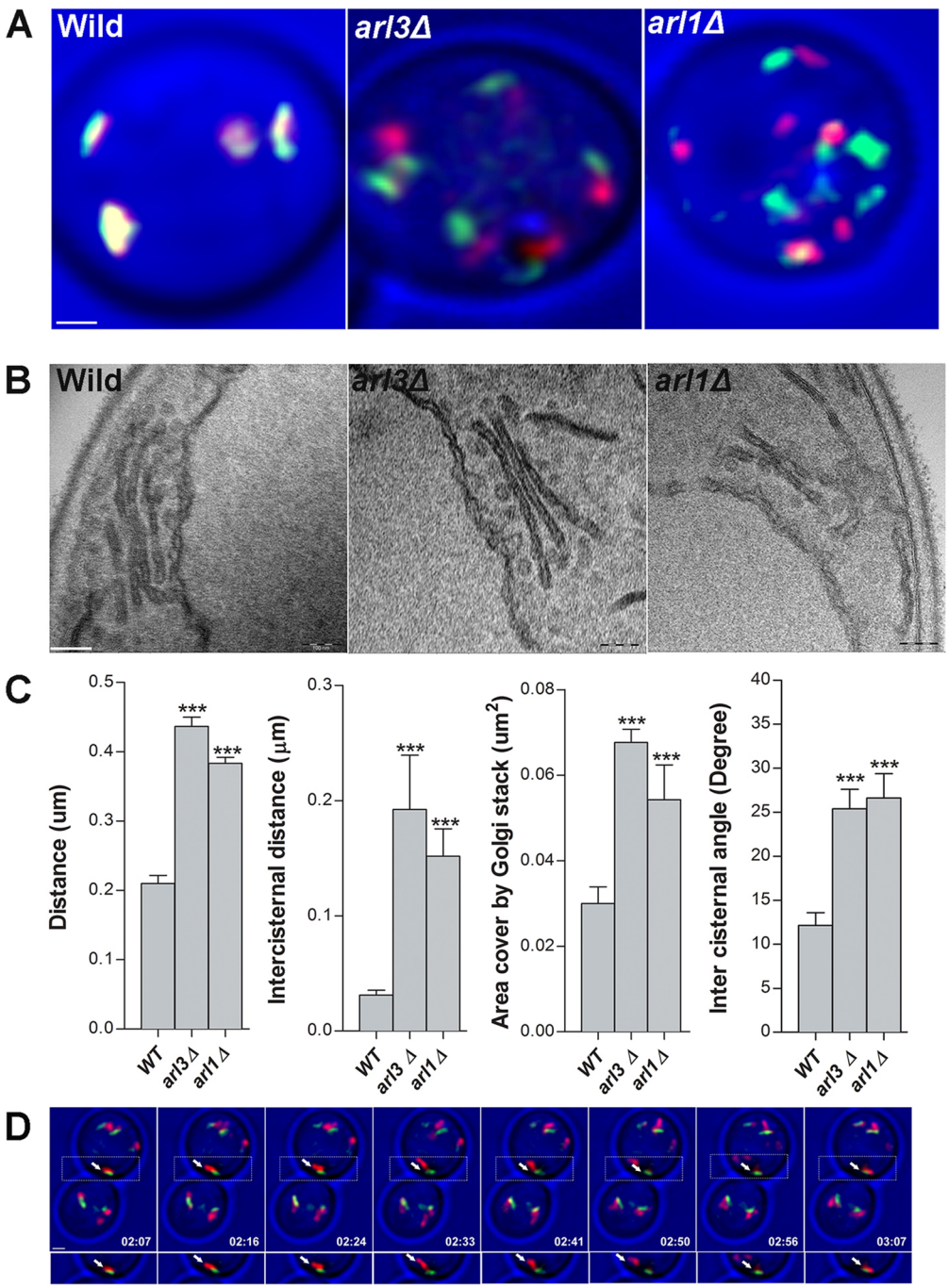

Fig. 4. The inter-cisternal distance increases in *arl3*Δ and *arl1*Δ cells, similar to what is seen in *Ppimh1*Δ cells. (A) *P. pastoris* strains expressing msGFP-*VIG4* and SEC7-DsRed.M1x6 were deleted for *arl3Δ* and *arl1Δ*. Cells were grown to log phase and imaged under a Leica SP8 confocal imaging system. Optical sections of 200 nm thickness were collected for the entire volume of cells. Image hyperstacks were deconvoluted using Huygens Pro and further filtered and *Z*-projected using ImageJ. Representative cells are shown. Scale bar: 1 µm. (B) Thin section electron micrograph of *P. pastoris* PPY12 wild-type, *arl3*Δ and *arl1*Δ cells. *P. pastoris* WT, *arl3Δ*, and *arl1Δ* cells were grown until log phase. Cells were concentrated, fixed and processed for thin section electron micrograph as described in the Materials and Methods. A representative cell is shown. Scale bar: 100 nm. (C) Left, the distance between the green and red spot from confocal microscopy images was measured using Imarisx64 8.0.1 Biplane. To quantitate the intercisternal distance, images were opened in Imaris, the surface was filled using 3D rendering for a specific channel, then the individual surface was considered as the solid object, and the center point was selected. By using the pointer, the distance between one green and one red spot was measured. Values represent mean±s.e.m. (*n*=60 cells) ***P<0.0002 (Student's) *t*-test. Quantitative data from thin section electrograph were measured using iTEM analysis software. The three panels on the right show, from left to right, the maximum inter-cisternal distance between two cisternae, the area covered by the entire Golgi stack and the angle between two cisternae. Values represent mean±s.e.m. (*n*=45 cells). ***P<0.0002 (Student's *t*-test). (D) A *P. pastoris Arl3* deletion strain expressing msGFP-*VIG4* and SEC7-DsRed.M1x6 was grown to the log phase. Live-cell 4D movies were captured using Leica SP8 with optical *z*-slice 0.3 nm, zoom factor 7 and 100× magnification. The typical 4D movie was deconvoluted using Huygens Pro software, and *Z*-projected using ImageJ. Scale bars: 1 µm. Frames from a representative 4D movie are shown (Movie 4). The arrow is marking the Golgi cisternal unstacking and stacking events. The time interval is in mm:ss. Enlarged views of corresponding frames from the live-cell 4D movie of *arl3*Δ cells are shown in the lower panel. The early Golgi marker is msGFP-*VIG4* and the late Golgi marker SEC7-DsRed.M1x6. The arrow is marking the Golgi cisternal unstacking and stacking event.

Journal of Cell Science (2019) 132, jcs230672. doi:10.1242/jcs.230672

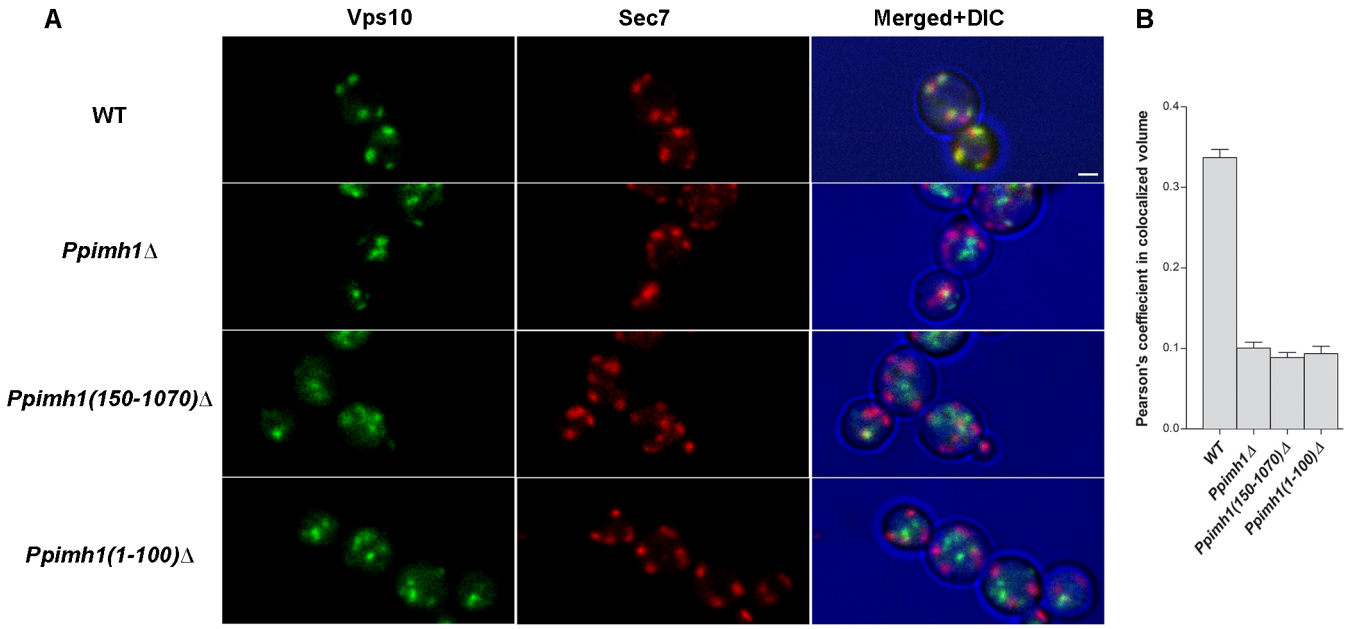

Fig. 5. The N-terminal 100 amino acids of *PpImh1* is essential for pre-vacuolar endosome to Golgi transport. (A) Wild-type (WT), *Ppimh1*Δ, *Ppimh1*(150-1070)Δ (lacking PpIm1h amino acids 150–1070) and *Ppimh1*(1-100)Δ (lacking PpImh1 amino acids 1–100) *P. pastoris* cells expressing SEC7–DsRed.M1x6 and Vps10–GFP were grown to log phase and imaged under the Leica SP8 system. Optical sections of 200 nm thickness were collected for the entire volume of cells. Image hyperstacks were deconvoluted using Huygens Pro and further filtered and *Z*-projected using ImageJ. Representative cells are shown. Scale bar: 1 µm. (B) Pearson's coefficient in colocalized volume was calculated from the images captured for *Ppimh1*Δ, *Ppimh1*(150-1070)Δ and *Ppimh1*(1-100)Δ strains tagged with SEC7-DsRed.M1x6 and Vps10-GFP. Values represent mean±s.e.m. (*n*=35).

capture of endosome-to-Golgi carriers in mammalian systems. (Wong et al., 2017; Cheung and Pfeffer, 2016).To validate whether the similar region of *Pp*Imh1 is functionally conserved or not, we deleted the N-terminal 100 amino acids of endogenous *Pp*Imh1. We observed that, in such strains, Vps10–GFP failed to localize in Golgi, suggesting that pre-vacuolar endosome to late Golgi vesicle capturing function is compromised (Fig. 5; Fig. S6A). These results further confirm that the deletion of only 1–100 amino acids residues of endogenous *Pp*Imh1 is sufficient to abolish the vesicle capture function of *Pp*Imh1.

Deletion of the coiled-coil domain of endogenous *Pp*Imh1 also abolished the vesicle capture function (Fig. 5). This suggests that both the N terminal domain (amino acids 1–100) and the coiled-coil domain are necessary for the vesicle capture function of *Pp*Imh1. We also tested the effect of the N-terminal deletion on the cisternal stacking phenotype by electron microscopy (Fig. 6C) and light microscopy (Fig. 6A). Surprisingly, this experiment revealed that there was no change in inter-cisternal distance and other parameters (Fig. 6B,D). This result suggests that the cisternal stacking function of *Pp*Imh1 is not dependent on its vesicle capturing function. However, the vesicle capturing function may be dependent on its stacking function, as the deletion of the coiled-coil domain (the essential domain for cisternal stacking function) also abolishes the vesicle capture function.

Golgi localization of *Pp*Imh1

GRIP domain golgins are known to localize in late Golgi/TGN. The GRIP domain of Golgin-97 is sufficient for the recruitment of Golgin-97 to the TGN (Munro and Nichols, 1999; Setty et al., 2003). To test what is the exact localization of *Pp*Imh1, we tagged *Pp*Imh1 with GFP and checked its localization with respect to early and late Golgi markers. GFP–*Pp*Imh1 was found to overlap with both cis-Golgi and late-Golgi markers (Fig. 6E). By measuring the percentage of the green spot that overlapped the red spot, we confirmed that it colocalized with both early and late Golgi (Fig. 6F). These results suggested to us that *Pp*Imh1 could be localized to the medial compartment. This result also fits well with our hypothesis that *Pp*Imh1 mediates the stacking between medial and late Golgi. We also observed that GFP–*Pp*Imh1 forms a ring-like pattern (Fig. 6E), with a central clearance and higher concentration of signal at the periphery. This suggests that *Pp*Imh1 may localize at the periphery of the Golgi cisterna to mediate cisternal stacking. To further analyze this, we compared the localization pattern of the Golgi-localizing GRIP domain (GFP–GRIP) and full-length *Pp*Imh1 tagged with GFP. GFP–*Pp*Imh1 showed an elongated ring-like the pattern, but in the case of the GRIP domain, we observed a punctate pattern (Fig. S7).

DISCUSSION

The role of golgins in maintaining Golgi structure has been experimentally shown previously (Nakamura et al., 1995; Slusarewicz et al., 1994; Waters et al., 1992; Derby et al., 2007; Lu et al., 2004), but, until now, there was not definitive proof of a direct role for any golgin in maintaining reversible cisternal stacking. Our results, for the first time, suggest that golgin *Pp*Imh1 knockout affect cisternal stacking between medial and late-Golgi. Moreover, the coiled-coil domain of golgin *Pp*Imh1 was shown to be essential for cisternal stacking. Our previous studies have shown that *Pp*Imh1 forms parallel homodimers where central coiled-coil domain remains in the dimeric state (Jain et al., 2018), suggesting that coiled-coil domain of golgin *Pp*Imh1 dimerizes and holds cisternae together. The results shown here support our hypothesis that the long coiled-coil domain could mediate dimerization of golgin molecules residing on two different Golgi cisterna and that multiple such dimerized golgin pairs could bring two Golgi cisternae together to form a stack. Our data suggest that *Pp*Imh1 mediates the cisternal stacking of late and medial Golgi. We also have shown that the Arl3–Arl1 GTPase cascade switch regulates this function. Our results suggest that the

Journal of Cell Science (2019) 132, jcs230672. doi:10.1242/jcs.230672

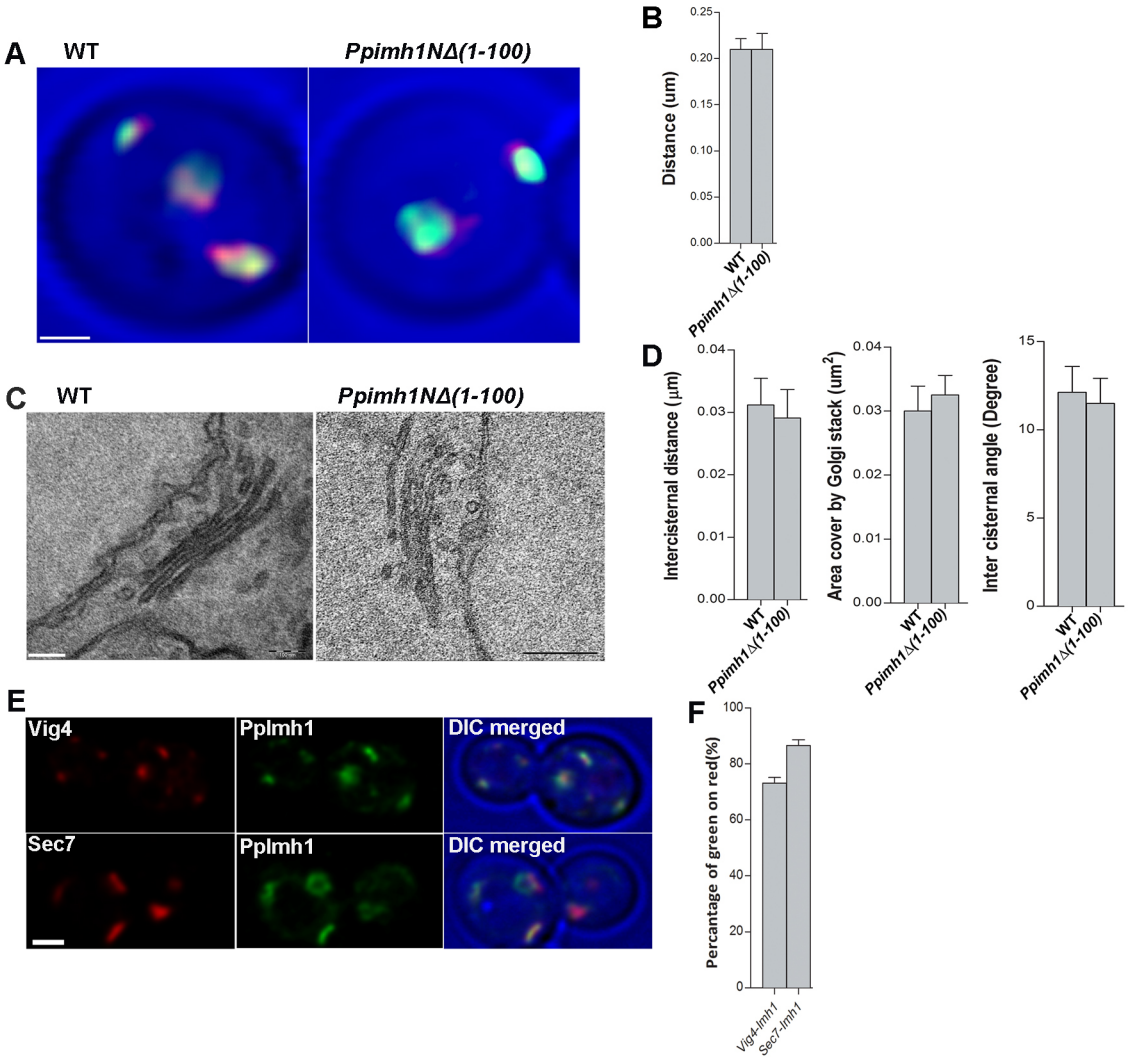

Fig. 6. Deletion of the N-terminal 100 amino acids region of *Pp*Imh1 does not affect Golgi cisternal stacking. (A) Wild-type (WT), and *Ppimh1*(1-100)Δ [*Ppimh1N*Δ(1-100); lacking PpImh1 amino acids 1–100] *P. pastoris* cells expressing msGFP-*VIG4* and SEC7-DsRed.M1x6 were grown to log phase, and images were captured under a Leica SP8 system. Optical sections of 200 nm thickness were collected for the entire volume of cells. Image hyperstacks was deconvoluted using Huygens Pro and further filtered and *Z*-projected using ImageJ. Representative cells are shown. Scale bar: 1 µm. (B) To quantify the intercisternal distance, the distance between the green and red spot were measured using Imaris Biplane. Values represent mean±s.e.m. (*n*=60 cells). (C) Thin section electron micrograph of *P. pastoris* PPY12 wild-type and *Ppimh1*(1-100)Δ cells were taken as described in the Materials and Methods. A representative cell is shown. Scale bars: 100 nm. (D) Quantitative data from thin section electrograph were measured using iTEM analysis software. Left, maximum intercisternal distance between two cisternae; middle, area covered by the entire Golgi stack; right, angle between two cisternae. Values represent mean±s.e.m. (*n*=45 cells). (E) Cells expressing GFP–*PpIMH1* were transformed with the cis-Golgi marker mcherry–*VIG4* and trans-Golgi marker SEC7-DsRed.M1x6. The resulting strains (GFP-*PpIMH1* mcherry-*VIG4* and GFP-*Pp*IMH1, SEC7DsRed.M1x6) were grown until log phase and images were taken under Leica SP8 confocal imaging system. Optical sections of 200 nm thickness were collected for the entire volume of cells. Image hyperstacks were deconvoluted using Huygens Pro and further filtered and Z-projected using ImageJ. Representative cells are shown. Scale bar: 1 µm. (F) The overlap between two differently labeled punctate compartments was quantified. Colocalization for each pair was measured as the percentage of the GFP signal that overlapped with a mask created from the mCherry–Vig4, and Sec7–6xDsRed.M1 signal. Colocalization of the two markers was determined using ImageJ (60 cells). Values represent mean±s.e.m. (*n*=60 cells).

GTP hydrolysis cycles of Arl proteins regulate the cycle of *Pp*Imh1 association and dissociation to Golgi cisterna and thereby function as an on-off switch for the stacking function of *Pp*Imh1 in a periodic manner; this, in turn, results in the reversible stacking.

Based on our results, we propose the following working model of *Pp*Imh1 on Golgi cisterna (Fig. 7A). First, GTP-Arl3 recruit Arl1, and as a result, *Pp*Imh1 associates to medial and late cisterna through its GRIP domain. As late cisterna matures to TGN, Arl3 goes through GTP hydrolysis and becomes GDP-Arl3. As a result, the GRIP domain anchor of *Pp*Imh1 dissociates from the maturing TGN. This, in turn, initiates the peeling of TGN. Eventually, the remaining anchor of the *Pp*Imh1 dimer dissociates from corresponding cisterna, as it matures, and the local GDP-Arl3 population increases. As a result, *Pp*Imh1 dimers dissociate, which in turn causes complete dissociation of the TGN from the Golgi stack. This separating form of TGN, also referred to as ffTGN, has been visualized experimentally to separate rapidly from the rest of the Golgi stack (Mogelsvang et al., 2003). As *Pp*Imh1 dimers dissociate from outgoing late compartments, new *Pp*Imh1 dimers reform, tethering between freshly matured medial and late cisterna with the progression of cisternal maturation. When *Pp*Imh1 is absent, functionally inactive or not recruited to the Golgi, the tethering between medial and late cisterna is lost. As a result, the

Journal of Cell Science (2019) 132, jcs230672. doi:10.1242/jcs.230672

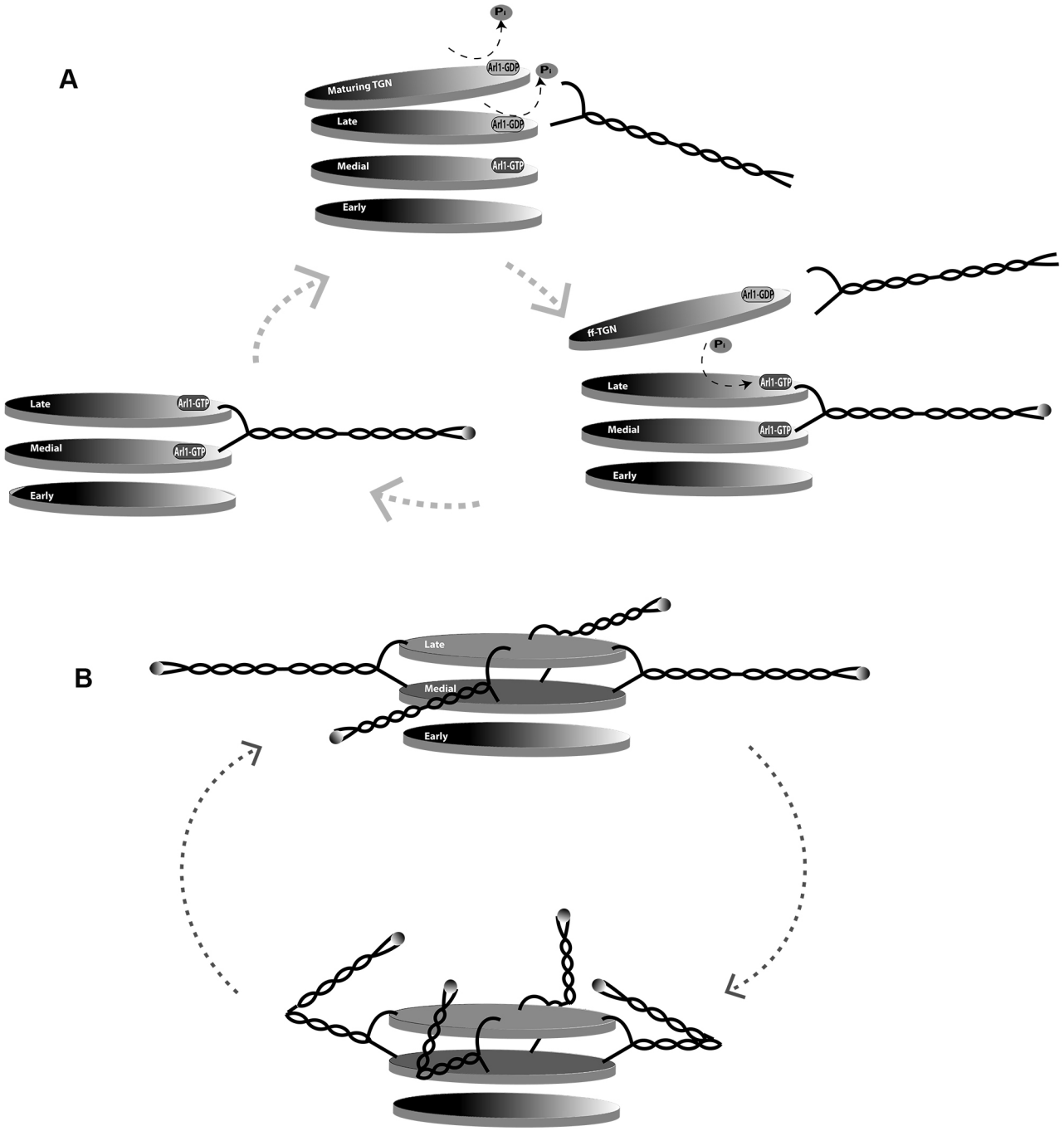

Fig. 7. Model suggesting the reversible cisternal stacking and putative dual function of *Pp*lmh1 – cisternal stacking and vesicle capture. (A) The Arl3–Arl1 GTPase cycle regulates the reversible cisternal stacking. Arl3-GDP convertsin to Arl3p-GTP through the action of an unknown GEF. Arl3-GTP then recruits a GEF which converts Arl1p-GDP into Arl1p-GTP, which recruits the GRIP domain-containing protein *Pp*lmh1 to the Golgi cisternae. Golgin molecules dimerize and mediate stacking between medial and trans-Golgi. Cisternal maturation of Golgi cisternae results in changes in membrane curvature which converts the Arl1-GTP form into Arl1-GDP and *Pp*lmh1 dissociates from the Golgi cisternae, and cisternae peel off from the Golgi stack. The continuous Arl3–Arl1 GTPase cycle regulates the cisternal stacking and maturation process. (B) This hypothetical model suggests the dual function of *Pplmh1*. The cisternal stacking function is mediated by anchoring the Golgi-localizing GRIP domain to Golgi cisterna and, utilizing coiled-coil dimerization, it brings two cisternae together and mediates cisternal stacking. The vesicle capture function is governed by capturing vesicle by N terminal head domain and, with the help of a hinge region, provides flexibility to Golgi cisterna for transporting vesicles.

late compartment, including the TGN peels off earlier and at a faster rate, as seen by Sec7-labeled compartments dynamics (Fig. 4D). The precise mechanism of the association–dissociation cycles of *Pp*Imh1 dimers to Golgi cisterna needs further investigation. It would be interesting to know whether the dissociating PpImh1 dimers are reformed or recycled.

One intriguing question is how the cell could ensure that only *Pp*Imh1 molecules residing on two neighboring cisternae can dimerize. It is possible that *Pp*Imh1 molecules residing on the same cisterna could also dimerize, but a significant number of *Pp*Imh1 molecules, enough to mediate reversible stacking, residing on two neighboring cisternae also dimerize. A mixed population of these

Journal of Cell Science (2019) 132, jcs230672. doi:10.1242/jcs.230672

two types of *Pp*Imh1 dimers (depending on their GRIP domain anchoring) possibly exists. Further investigations will decipher the actual ratio of these two population at a given time.

The established function of golgins is to capture vesicles coming from the different region of the cells. The GRIP domain golgins GCC185, Golgin-97 and Golgin-245 capture vesicles coming from the endosome and transfers them to the trans Golgi (Derby et al., 2007; Lieu et al., 2007; Lu et al., 2004). Our results support that golgin *Pp*Imh1 mediates transport vesicles between endosome and the TGN. The GRIP domain golgin GCC185 forms a Y-shaped structure where the N-terminal domain forms a splayed end, which has been shown to be essential for vesicle capture (Cheung et al., 2015; Wong et al., 2017). The golgin *Pp*Imh1 forms a parallel homodimer with a splayed N terminus (Jain et al., 2018). Our data further support that the N-terminal domain of *Pp*Imh1 is essential for the vesicle capture function of golgin *Pp*Imh1.

It appears that the cisternal stacking function of *Pp*Imh1 is independent of its vesicle capturing function since deletion of the vesicle capture domain *Pp*Imh1 (amino acids 1–100) had no effect on Golgi cisternal stacking. However, the deletion of the coiled-coil domain, which is essential for cisternal stacking, affects the vesicle capture function. That suggests that stacking could be indispensable for the vesicle capture function. However, it is also possible that deletion of coiled-coil domain results in reduction in the length of golgin molecule and this leads to the failure to capture the incoming vesicle. It is to be noted that the central coiled-coil domain is possibly necessary but not sufficient to confer the cisternal stacking function. Only the coiled-coil domain, along with the GRIP domain, is sufficient for cisternal stacking function (Fig. 6C). Our result also suggests that for thevesicle capture function *Pp*Imh1 needs all its three domains, that is, the N-terminal domain, coiled-coil domain and GRIP domain (Fig. 5). Since the deletion of the N-terminal domain (amino acids 1–100) compromises vesicle capture, and the same domain has been previously shown to form the splayed N-terminal Y -shaped structure suitable for vesicle capture, most likely this region is essential for vesicle capture. However, this region is dispensable for cisternal stacking (Fig. 6C). We hypothesize that cisternal stacking is independent of vesicle capturing functions, but the efficacy of the latter may be dependent on the former, which possibly enhance the robustness of the secretory function of the Golgi.

However, a natural question arises about how *Pp*Imh1 can accommodate these two separate functions simultaneously. We have accommodated this in our model (Fig. 7B). For the vesicle capturing function, the Y-shaped N-terminal regions of golgin dimers are a favored structure in which the splayed N-terminal of dimers are proposed to mediated interaction with the vesicles (Wong et al., 2017; Cheung et al., 2015). We have shown that the N-terminal domain of *Pp*Imh1 is essential for vesicle capture. The C-terminal domains of the *Pp*Imh1 dimers anchor the Golgi membrane of neighboring cisterna in a manner mediated by Arl1 interaction. The coiled-coil region of *Pp*Imh1 contains certain 'break' regions which possibly form hinge region that can provide flexibility to golgin molecule to allow vesicle transport to the Golgi membrane (Cheung et al., 2015). The *Pp*Imh1Y-shaped N-terminal dimer keeps on engaging in vesicle transport, while GRIP domain anchors mediate the stacking, as described above.

Our results suggest the possible role of GRIP domain golgins in Golgi stacking and vesicle capture. It seems likely that Golgi stacking involves multiple types of interactions. For the early Golgi, the mechanisms might vary between species, with GRASPs being one set of players in animal cells. By contrast, the GRIP domain-mediated reversible stacking mechanism might be conserved at the level of the late Golgi since various species have displayed a 'TGN peeling' phenotype (Mogelsvang et al., 2003; Mollenhauer and Morré, 1991). Moreover, GRIP domain proteins are conserved in plants, animals and fungi, so it is plausible that this mechanism of reversible Golgi stacking is evolutionarily conserved. Our studies provide a potential molecular basis for the 'TGN peeling off' phenomenon that has been seen by EM for decades.

MATERIALS AND METHODS

Experiments with *P. pastoris* were carried out using the haploid wild-type strain PPY12 (*his4 arg4*) (Gould et al., 1992) and its derivatives (Table S2). General methods for the growth and transformation of *P. pastoris* were as described previously (Sears et al., 1998). Cultures were grown in rich glucose medium (YPD), synthetic glucose medium (SD), or nonfluorescent synthetic glucose medium (NSD) (Bevis et al., 2002) in baffled flasks at 30°C with shaking at 200 rpm. Selection of strains were carried out on YPD supplemented with G418 (500 µg/ml) or Hygromycin B (250 µg/ml) or SD medium as per integrating plasmids. *P. pastoris* transformation was performed with linearized integrating vectors using the electroporation method. *P. pastoris* gene sequences were obtained from the NCBI database. Molecular biology procedures were simulated and recorded using SnapGene software. All plasmids and primers used in this study are listed in Tables S1 and S3.

P. pastoris expression and cell lysis

The *P. pastoris* yeast strain expressing *Pp*-GRIP and *Pp*-CC were grown to log phase [0.5 optical density at 600 nm (OD_{600})] in SYG medium (0.67% yeast nitrogen base, 0.05% yeast extract, 0.4 mg/l biotin, 40 mg/l arginine hydrochloride and 1% glycerol). Then cells were washed with SYM medium (0.67% yeast nitrogen base, 0.05% yeast extract, 0.4 mg/l biotin, 40 mg/l arginine hydrochloride and 1% methanol), and resuspended in SYM medium for 8 h to induce expression from the *AOX1* promoter. The cell pellet was washed with water and lysed with breaking buffer (50 mM sodium phosphate buffer, pH 7.4, 1 mM PMSF, 1 mM EDTA and 5% glycerol) and acid-washed glass beads as per the Invitrogen *Pichia* expression kit protocol. The cell lysate was mixed with 2× SDS gel loading dye. The protein samples were separated by SDS-PAGE and immunoblotted with anti-His antibody (1:3000; ab18184, Abcam, Cambridge, MA,).

Construction of a strain expressing tagged *VIG4*

Full-length *P. pastoris* VIG4 were PCR amplified. The amplified fragments were digested with EcoRI and SphI and ligated into the pIB1 (Sears et al., 1998) cut with the same enzyme. This plasmid was then mutagenized to introduce NotI and BamHI. The resulting plasmid was digested with NotI and BamHI and the fluorescent protein msGFP was inserted at NotI and BamHI site resulting in the msGFP-*VIG4*-pIB1 construct. This construct was linearized with StuI to integrate at *his4* locus of *P. pastoris*.

Construction of strain expressing tagged *SEC7*

SEC7 was epitope tagged with a 6X-DsRed.M1 (Bevis et al., 2002) cassette by pop-in gene replacement using the same general strategy as described above for *VIG4*. The pop-in plasmid pUC19-ARG4(-XmnI)-Pp*SEC7*-DsRed.M1×6 was linearized with XmnI for transformation into an *arg4* strain.

Knockout of *PpIMH1* in *P. pastoris*

1-kb sequences flanking the *PpIMH1* coding sequence were amplified from genomic DNA. The amplified fragments were digested with NdeI and SalI (for the upstream fragment) and XhoI and HpaI (for the downstream fragment). The upstream fragment was ligated with a pUG6 (Guldener et al., 1996) vector that had been digested with NdeI and SalI. The resulting plasmid was cut with XhoI and HpaI to ligate downstream fragment to give pUG6-*PpIMH1*::Kanmax. Finally, a 3.2-kb NdeI-HpaI fragment was excised from this plasmid and transformed into PPY12 cells. G418-resistant transformants were screened by PCR to confirm that *IMH1* had been deleted. Full-length *PpIMH1* was PCR amplified. The amplified fragment was digested with XmaI and SphI and ligated with pIB1

Journal of Cell Science (2019) 132, jcs230672. doi:10.1242/jcs.230672

(Sears et al., 1998) cut with the same enzyme. The resultant plasmid was linearized with StuI to integrate at the *His4* locus.

Construction of a strain expressing tagged *Pp*Imh1

Full-length *PpIMH1* was PCR amplified. The amplified fragment was digested with XmaI and SphI and ligated with the pUC19-His (Connerly et al., 2005) cut with the same enzyme. This plasmid was then mutagenized to introduce BamHI-NotI sites. The resulting plasmid was then digested with BamHI and NotI, and the GFP tag was ligated as a BamHI–NotI fragment. The GFP-*Pp*IMH1-pUC19-His construct was linearized with PstI to integrate at *PpIMH1* locus of *P. pastoris.*

Knockout of ARL3 in *P. pastoris*

1-kb sequences flanking the *ARL3* coding sequence were amplified from genomic DNA. The amplified fragments were digested with NdeI and SalI (for the upstream fragment) and SacII and HpaI (for the downstream fragment). The upstream fragment was ligated with pUG6 (Guldener et al., 1996) vector, which had been digested with NdeI and SalI. The resulting plasmid was cut with SacII and HpaI to ligate the downstream fragment, resulting in pUG6-*ARL3*: Kanmax. Finally, a 3.2-kb NdeI–HpaI fragment was excised from this plasmid and transformed into PPY12 cells. G418-resistant transformants were screened by PCR to confirm that *ARL3* had been deleted.

Knockout of Arl1 in *P. pastoris*

1-kb sequences flanking the *ARL1* coding sequence were amplified from genomic DNA. The amplified fragments were digested with NdeI and SalI (for the upstream fragment) and EcoRV and NotI (for the downstream fragment). The upstream fragment was ligated with a pUG6 (Guldener et al., 1996) vector that had been digested with NdeI and SalI. The resulting plasmid was cut with EcoRV and NotI to ligate downstream fragment that results in pUG6-*ARL1*:Kanmax. Finally, a 3.2-kb NdeI–NotI fragment was excised from this plasmid and transformed into PPY12 cells. G418-resistant transformants were screened by PCR to confirm that *ARL1* had been deleted.

Deletion of *Pp*Imh1 residues 1–100 and 150–1070

The open reading frame of the *P. pastoris IMH1* coiled-coil domain was deleted as follows. The sequence upstream of the *PpIMH1* coiled-coil domain (150–1070) and *PpIMH1* (1–100) coding region were amplified from genomic DNA. The amplified fragments were digested with SmaI and BamHI and ligated with a pUC19-His (Connerly et al., 2005) vector that had been digested with SmaI and BamHI. The resulting plasmid was cut with BamHI and SphI to ligate downstream fragments to result in pUC19-*PpIMH1*(150-1070)Δ and *PpIMH1(1-100)*Δ. These constructs were linearized with EcoRI and PstI to integrate at *PpIMH1* locus of *P. pastoris*.

Construction of strain expressing tagged Vps10

A 3′ portion of the *P. pastoris VPS10* coding sequence plus a downstream region were amplified by PCR. The amplified fragment was digested with EcoRI and HindIII and ligated with the pUC19-Arg4 cut with the same enzyme. This plasmid was then mutagenized to introduce BamHI-NotI sites. The resulting plasmid was then digested with BamHI and NotI, and a 3×GFP tag was ligated as a BamHI–NotI fragment. The Vps10-3×GFP-pUC19Arg4 construct was linearized with NsiI to integrate at *VPS10* locus of *P. pastoris.*

Construction of strain expressing tagged Vps8

A 3′ portion of the *P. pastoris VPS8* coding sequence plus a downstream region were amplified by PCR. The amplified fragment was digested with EcoRI and SphI and ligated with the pUC19-Arg cut with the same enzyme. This plasmid was then mutagenized to introduce BamHI-NotI sites. The resulting plasmid was then digested with BamHI and NotI, and the 3xGFP tag was ligated as a BamHI-NotI fragment. The Vps8-3xiGFP-pUC19Arg construct was linearized with BspEI to integrate at *VPS8* locus of *P. pastoris*

Fluorescence microscopy

Live-cell dual-color 4D confocal imaging was performed previously described (Day et al., 2017) using a strain expressing GFP–Vig4 as an early Golgi marker and Sec7–DsRed as a late Golgi marker, with the following modifications. Cells attached to the cover glass dish surface were washed and covered with minimal SD medium. Image capture was performed using a Zeiss 780 and Leica SP8 confocal microscope. GFP fluorescence was visualized using 488-nm laser light source excitation and 495–550 nm bandpass emission, and DsRed fluorescence was visualized using 561-nm excitation and 580–750 nm bandpass emission. The pixel size was 65 nm, the pinhole size was 1.2 Airy units, and the interval between the optical sections was 0.3 µm. Every 10 s, 20 optical sections were captured to span the entire cell thickness. The red and green fluorescence images were converted to 16-bit and average projected, then range-adjusted to the minimum and maximum pixel values in ImageJ, and merged with blue images of the cells.

4D imaging was performed using Leica SP8 with an optical *z* slice of 0.3 nm, zoom factor 7, and 100× objective magnification. The 4D movies were deconvoluted using Huygens Pro software, and *Z* projected using ImageJ. The entire event of TGN peeling was measured by analyzing the 10-min live-cell movies.

FM 4-64 labeling

FM 4-64 labeling of PVE or endosome was performed as described previously (Vida and Emr, 1995). Cells were grown to log phase; then, 1 ml of log-phase cells were suspended in YPD medium containing 1.6 µM FM 4-64 dye (Life Technologies, Carlsbad, CA) and incubated for 10 min at 30°C. Cells were washed and resuspended in 5 ml YPD and chased for 20 min at at 30°C and immediately observed under the microscope by spotting on the coverslip. To chase FM 4-64 in Sec7- and Vps8-tagged strains, cells were grown to log phase and incubated with FM 4-64 dye for 10 min. Cells were washed with YPD and chased for 3 min, 10 min, 15 min or 20 min.

Quantification of colocalization

The overlap between two differently labeled punctate compartments was quantified as described previously (Levi et al., 2010). The fraction of the GFP–*Pp*Imh1 punctate signal that overlapped with the red Golgi marker punctate signal was quantified in ImageJ. The red and green channels from a merged RGB image were separated in Photoshop (Adobe), converted into grayscale, inverted to give dark spots on a light background, processed with the Despeckle filter and saved as separate TIFF files. The TIFF file for the corresponding channel was then opened in ImageJ, and a binary threshold image of black spots on a white background was created using the Dynamic threshold 1d plug-in; a similar procedure was used to generate a modified TIFF file displaying only the punctate spots from the green channel. The total signals from the red and green spots were then obtained using the Measure command in ImageJ. To determine the fraction of the punctate red signal that overlapped with the punctate green signal, the binary threshold image from the green channel was subtracted from the TIFF file for the red channel. The resulting signal was measured and was divided by the total signal previously measured for the red spots.

Electron microscopy

Thin-section EM was performed essentially as described previously (Gould et al., 1992). In brief, a 50-ml culture of yeast cells in rich glucose medium was grown to an OD_{600} of ∼0.5. The culture was concentrated to a volume of <5 ml with a bottle-top vacuum filter, and 40 ml of ice-cold 50 mM potassium phosphate buffer, pH 6.8, 1 mM $MgCl_2$ and 2% glutaraldehyde was added rapidly with swirling. After fixation for 1 h on ice, the cells were washed repeatedly, and then resuspended in 0.75 ml 4% $KMnO_4$ and mixed for 1 h at room temperature. The cells were washed, and then resuspended in 0.75 ml 2% uranyl acetate and mixed for 1 h at room temperature. Finally, the cells were embedded in Spurr's resin; 50 ml of yeast culture yielded enough cells for three BEEM capsules. The resin was polymerized for 2 days at 68°C. Sections were stained with uranyl acetate and lead citrate and viewed on an electron microscope (100 CXII; JEOL Inc). All the parameters were measured using iTEM analysis software.

Statistical analysis

Three independent experiments were performed to capture fluorescence and electron microscopy images. In each experiment, 20 images were captured. The total number of images used for analysis are given as '*n*' values in the legend. An unpaired Student's *t*-test was performed to assess the statistical significances of differences among datasets. Two-tailed unpaired Student's *t*-tests were performed using GraphPad Prism. $P<0.05$ was considered statistically significant.

Acknowledgements

We thank Prof. Benjamin Glick of the University of Chicago for his various inputs and his critical comments for the preparation of the manuscript. We also thank all the Bhattacharyya lab members for carefully reviewing the manuscript.

Competing interests

The authors declare no competing or financial interests.

Author contributions

Conceptualization: D.B.; Methodology: B.K.J., R.D., D.B.; Validation: B.K.J., R.D.; Formal analysis: B.K.J.; Investigation: B.K.J., D.B.; Data curation: B.K.J., R.D., D.B.; Writing - original draft: D.B.; Writing - review & editing: D.B.; Visualization: B.K.J., D.B.; Supervision: D.B.; Project administration: D.B.; Funding acquisition: D.B.

Funding

This work was supported by funding from Department of Biotechnology, Ministry of Science and Technology (DBT; Government of India) [DBT grant BT/PR14909/BRB/10/887/2010 (to D.B)] and an Advanced Centre for Treatment, Research and Education in Cancer (ACTREC) doctoral fellowship through HBNI to B.K.J.

Supplementary information

Supplementary information available online at
http://jcs.biologists.org/lookup/doi/10.1242/jcs.230672.supplemental

References

Alzhanova, D. and Hruby, D. E. (2006). A trans-Golgi network resident protein, golgin-97, accumulates in viral factories and incorporates into virions during poxvirus infection. *J. Virol.* **80**, 11520-11527. doi:10.1128/JVI.00287-06

Bekier, M. E., II, Wang, L., Li, J., Huang, H., Tang, D., Zhang, X. and Wang, Y. (2017). Knockout of the Golgi stacking proteins GRASP55 and GRASP65 impairs Golgi structure and function. *Mol. Biol. Cell* **28**, 2833-2842. doi:10.1091/mbc.e17-02-0112

Bevis, B. J., Hammond, A. T., Reinke, C. A. and Glick, B. S. (2002). De novo formation of transitional ER sites and Golgi structures in Pichia pastoris. *Nat. Cell Biol.* **4**, 750-756. doi:10.1038/ncb852

Bhave, M., Papanikou, E., Iyer, P., Pandya, K., Jain, B. K., Ganguly, A., Sharma, C., Pawar, K., Austin, J., II, Day, K. J. et al. (2014). Golgi enlargement in Arf-depleted yeast cells is due to altered dynamics of cisternal maturation. *J. Cell Sci.* **127**, 250-257. doi:10.1242/jcs.140996

Burguete, A. S., Fenn, T. D., Brunger, A. T. and Pfeffer, S. R. (2008). Rab and Arl GTPase family members cooperate in the localization of the golgin GCC185. *Cell* **132**, 286-298. doi:10.1016/j.cell.2007.11.048

Cheung, P.-Y. P. and Pfeffer, S. R. (2016). Transport vesicle tethering at the trans golgi network: coiled coil proteins in action. *Front Cell Dev. Biol.* **4**, 18. doi:10.3389/fcell.2016.00018

Cheung, P.-Y. P., Limouse, C., Mabuchi, H. and Pfeffer, S. R. (2015). Protein flexibility is required for vesicle tethering at the Golgi. *eLife* **4**, e12790. doi:10.7554/eLife.12790

Connerly, P. L., Esaki, M., Montegna, E. A., Strongin, D. E., Levi, S., Soderholm, J. and Glick, B. S. (2005). Sec16 is a determinant of transitional ER organization. *Curr. Biol.* **15**, 1439-1447. doi:10.1016/j.cub.2005.06.065

Cooper, A. A. and Stevens, T. H. (1996). Vps10p cycles between the late-Golgi and prevacuolar compartments in its function as the sorting receptor for multiple yeast vacuolar hydrolases. *J. Cell Biol.* **133**, 529-541. doi:10.1083/jcb.133.3.529

Day, K. J., La Rivière, P. J., Chandler, T., Bindokas, V. P., Ferrier, N. J. and Glick, B. S. (2017). Improved deconvolution of very weak confocal signals. *F1000Res* **6**, 787. doi:10.12688/f1000research.11773.1

Day, K. J., Casler, J. C. and Glick, B. S. (2018). Budding yeast has a minimal endomembrane system. *Dev. Cell* **44**, 56-72.e4. doi:10.1016/j.devcel.2017.12.014

Derby, M. C., Lieu, Z. Z., Brown, D., Stow, J. L., Goud, B. and Gleeson, P. A. (2007). The trans-Golgi network golgin, GCC185, is required for endosome-to-Golgi transport and maintenance of Golgi structure. *Traffic* **8**, 758-773. doi:10.1111/j.1600-0854.2007.00563.x

Gould, S. J., Mccollum, D., Spong, A. P., Heyman, J. A. and Subramani, S. (1992). Development of the yeast Pichia pastoris as a model organism for a genetic and molecular analysis of peroxisome assembly. *Yeast* **8**, 613-628. doi:10.1002/yea.320080805

Guldener, U., Heck, S., Fielder, T., Beinhauer, J. and Hegemann, J. H. (1996). A new efficient gene disruption cassette for repeated use in budding yeast. *Nucleic Acids Res.* **24**, 2519-2524. doi:10.1093/nar/24.13.2519

Ito, Y., Uemura, T. and Nakano, A. (2014). Formation and maintenance of the Golgi apparatus in plant cells. *Int. Rev. Cell Mol. Biol.* **310**, 221-287. doi:10.1016/B978-0-12-800180-6.00006-2

Iyer, P., Bhave, M., Jain, B. K., Roychowdhury, S. and Bhattacharyya, D. (2018). Vps74p controls Golgi size in an Arf1-dependent manner. *FEBS Lett.* **592**, 3720-3735. doi:10.1002/1873-3468.13266

Jain, B. K., Thapa, P. S., Varma, A. and Bhattacharyya, D. (2018). Identification and characterization of GRIP domain Golgin PpImh1 from Pichia pastoris. *Yeast* **35**, 499-506. doi:10.1002/yea.3317

Lee, I., Tiwari, N., Dunlop, M. H., Graham, M., Liu, X. and Rothman, J. E. (2014). Membrane adhesion dictates Golgi stacking and cisternal morphology. *Proc. Natl. Acad. Sci. USA* **111**, 1849-1854. doi:10.1073/pnas.1323895111

Levi, S. K., Bhattacharyya, D., Strack, R. L., Austin, J. R., II and Glick, B. S. (2010). The yeast GRASP Grh1 colocalizes with COPII and is dispensable for organizing the secretory pathway. *Traffic* **11**, 1168-1179. doi:10.1111/j.1600-0854.2010.01089.x

Lieu, Z. Z., Derby, M. C., Teasdale, R. D., Hart, C., Gunn, P. and Gleeson, P. A. (2007). The golgin GCC88 is required for efficient retrograde transport of cargo from the early endosomes to the trans-Golgi network. *Mol. Biol. Cell* **18**, 4979-4991. doi:10.1091/mbc.e07-06-0622

Losev, E., Reinke, C. A., Jellen, J., Strongin, D. E., Bevis, B. J. and Glick, B. S. (2006). Golgi maturation visualized in living yeast. *Nature* **441**, 1002-1006. doi:10.1038/nature04717

Lowe, M. (2011). Structural organization of the Golgi apparatus. *Curr. Opin. Cell Biol.* **23**, 85-93. doi:10.1016/j.ceb.2010.10.004

Lu, L. and Hong, W. (2003). Interaction of Arl1-GTP with GRIP domains recruits autoantigens Golgin-97 and Golgin-245/p230 onto the Golgi. *Mol. Biol. Cell* **14**, 3767-3781. doi:10.1091/mbc.e03-01-0864

Lu, L., Tai, G. and Hong, W. (2004). Autoantigen Golgin-97, an effector of Arl1 GTPase, participates in traffic from the endosome to the trans-golgi network. *Mol. Biol. Cell* **15**, 4426-4443. doi:10.1091/mbc.e03-12-0872

Marcusson, E. G., Horazdovsky, B. F., Cereghino, J. L., Gharakhanian, E. and Emr, S. D. (1994). The sorting receptor for yeast vacuolar carboxypeptidase Y is encoded by the VPS10 gene. *Cell* **77**, 579-586. doi:10.1016/0092-8674(94)90219-4

Mogelsvang, S., Gomez-Ospina, N., Soderholm, J., Glick, B. S. and Staehelin, L. A. (2003). Tomographic evidence for continuous turnover of Golgi cisternae in Pichia pastoris. *Mol. Biol. Cell* **14**, 2277-2291. doi:10.1091/mbc.e02-10-0697

Mollenhauer, H. H. and Morré, D. J. (1991). Perspectives on Golgi apparatus form and function. *J. Electron. Microsc. Tech.* **17**, 2-14. doi:10.1002/jemt.1060170103

Munro, S. and Nichols, B. J. (1999). The GRIP domain - a novel Golgi-targeting domain found in several coiled-coil proteins. *Curr. Biol.* **9**, 377-380. doi:10.1016/S0960-9822(99)80166-3

Nakamura, N., Rabouille, C., Watson, R., Nilsson, T., Hui, N., Slusarewicz, P., Kreis, T. E. and Warren, G. (1995). Characterization of a cis-Golgi matrix protein, GM130. *J. Cell Biol.* **131**, 1715-1726. doi:10.1083/jcb.131.6.1715

Nakamura, N., Wei, J.-H. and Seemann, J. (2012). Modular organization of the mammalian Golgi apparatus. *Curr. Opin. Cell Biol.* **24**, 467-474. doi:10.1016/j.ceb.2012.05.009

Panic, B., Perisic, O., Veprintsev, D. B., Williams, R. L. and Munro, S. (2003). Structural basis for Arl1-dependent targeting of homodimeric GRIP domains to the Golgi apparatus. *Mol. Cell* **12**, 863-874. doi:10.1016/S1097-2765(03)00356-3

Papanikou, E. and Glick, B. S. (2009). The yeast Golgi apparatus: insights and mysteries. *FEBS Lett.* **583**, 3746-3751. doi:10.1016/j.febslet.2009.10.072

Ramirez, I. B.-R. and Lowe, M. (2009). Golgins and GRASPs: holding the Golgi together. *Semin. Cell Dev. Biol.* **20**, 770-779. doi:10.1016/j.semcdb.2009.03.011

Sears, I. B., O'connor, J., Rossanese, O. W. and Glick, B. S. (1998). A versatile set of vectors for constitutive and regulated gene expression in Pichia pastoris. *Yeast* **14**, 783-790. doi:10.1002/(SICI)1097-0061(19980615)14:8<783::AID-YEA272>3.0.CO;2-Y

Setty, S. R. G., Shin, M. E., Yoshino, A., Marks, M. S. and Burd, C. G. (2003). Golgi recruitment of GRIP domain proteins by Arf-like GTPase 1 is regulated by Arf-like GTPase 3. *Curr. Biol.* **13**, 401-404. doi:10.1016/S0960-9822(03)00089-7

Slusarewicz, P., Nilsson, T., Hui, N., Watson, R. and Warren, G. (1994). Isolation of a matrix that binds medial Golgi enzymes. *J. Cell Biol.* **124**, 405-413. doi:10.1083/jcb.124.4.405

Vida, T. A. and Emr, S. D. (1995). A new vital stain for visualizing vacuolar membrane dynamics and endocytosis in yeast. *J. Cell Biol.* **128**, 779-792. doi:10.1083/jcb.128.5.779

Waters, M. G., Clary, D. O. and Rothman, J. E. (1992). A novel 115-kD peripheral membrane protein is required for intercisternal transport in the Golgi stack. *J. Cell Biol.* **118**, 1015-1026. doi:10.1083/jcb.118.5.1015

Wong, M., Gillingham, A. K. and Munro, S. (2017). The golgin coiled-coil proteins capture different types of transport carriers via distinct N-terminal motifs. *BMC Biol.* **15**, 3. doi:10.1186/s12915-016-0345-3

Wu, M., Lu, L., Hong, W. and Song, H. (2004). Structural basis for recruitment of GRIP domain golgin-245 by small GTPase Arl1. *Nat. Struct. Mol. Biol.* **11**, 86-94. doi:10.1038/nsmb714

Yoshino, A., Bieler, B. M., Harper, D. C., Cowan, D. A., Sutterwala, S., Gay, D. M., Cole, N. B., Mccaffery, J. M. and Marks, M. S. (2003). A role for GRIP domain proteins and/or their ligands in structure and function of the trans Golgi network. *J. Cell Sci.* **116**, 4441-4454. doi:10.1242/jcs.00746

Zhang, X. and Wang, Y. (2015). GRASPs in Golgi structure and function. *Front. Cell Dev. Biol.* **3**, 84. doi:10.3389/fcell.2015.00084